ACS OMEGA

http://pubs.acs.org/journal/acsodf

Article

Numerical Simulation Study on Flow and Heat Transfer of the Tungsten Crucible CVD Reactor

Lipei Peng, Han Dong,* Shaobo Li, Zhanwei Wang, Xiangjun Meng, Yafeng Wang, Tengshi Liu, Xiangyu Li, and Jialiang Ji

Cite This: *ACS Omega* 2022, 7, 42044−42055

Read Online

ACCESS | Metrics & More | Article Recommendations

ABSTRACT: In order to investigate the optimization of the performance and structure of a tungsten crucible CVD reactor, the CFD simulation method was used in this paper to simulate the internal flow of the tungsten crucible CVD reactor. The velocity distribution and temperature distribution in the reactor were obtained. The simulation results show that the axial and radial heat convection will occur between the susceptor and the outer wall surface, but the axial heat convection is more intense. Moreover, it was found that the temperature distribution in the CVD reactor was more uniform and reasonable when the upper gas inlet was applied, which was beneficial to the reduction and deposition processes of tungsten. The molar ratio of H_2 to WF_6 has a great influence on the deposition rate of tungsten, and excess H_2 is not conducive to the deposition of tungsten. Thermal radiation has a great influence on the temperature distribution of CVD reactors. It cannot be neglected.

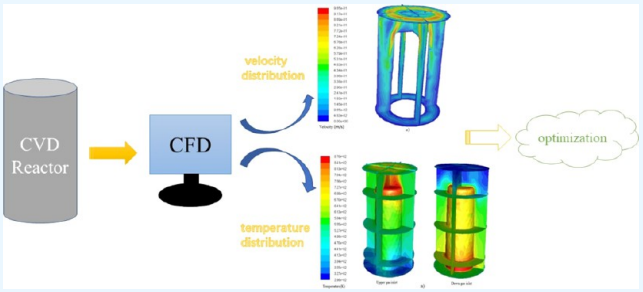

1. INTRODUCTION

The chemical vapor deposition (CVD) process can complete material preparation at low temperatures and achieve material growth in accordance with set chemical composition measurement ratio on a microscale. It is widely used in the preparation field of functional materials.[1] The preparation of metal tungsten coating and special-shaped products by CVD method can easily and directly obtain high-density and high-purity tungsten coating and parts, especially for the preparation of high-purity tungsten coating, complex shape, small-size special-shaped parts, and so forth, which has great advantages.[2−4] As tungsten and its alloys have become one of the most important functional materials in modern industry, national defense, and high and new technology and are widely used in aerospace, atomic energy, nuclear power, ships, weapons, automobiles, electrical, electronics, chemistry, metallurgy, machinery, and other fields.[5−8] The preparation of tungsten products by the CVD method has attracted people's attention.

In the late 1980s, it was reported that hydrogen was used to reduce tungsten hexafluoride to prepare the special-shaped metal tungsten products with high density and purity.[9−11] However, these reports have little influence on the microstructures, structures, and properties of tungsten coating by the specific process and the temperature distribution inside a reactor. At present, more and more scholars have studied the CFD simulation of a CVD reactor,[12−16] but few have studied the CFD simulation of a tungsten CVD reactor.

2. NUMERICAL METHOD

The flow and heat transfer in the tungsten crucible CVD reactor have been numerically simulated. Tungsten deposition is a gas-phase reaction process. The gas-phase reaction is an inhomogeneous reaction in which gases react to form metals. The reaction process can be divided into three steps. The first step is the diffusion of the reaction gas to the surface of the susceptor and the diffusion of the byproduct from the reaction zone. The rate of these processes is mainly determined by hydrodynamic factors. The second step is the diffusion of the initial reactants and gas products through the boundary layer. The rate of this reaction is determined by physical factors and the thickness of the surface layer, depending on the surface roughness and the nature of the reaction airflow. The third step is the adsorption of molecules on the surface of the susceptor, which is accompanied by the chemical reaction, adsorption, and desorption of reaction products. These processes are closely linked and inseparable. However, in order to reduce the difficulty of simulation calculation, the reaction process was reasonably simplified in this study. The

Received: June 28, 2022
Accepted: October 31, 2022
Published: November 8, 2022

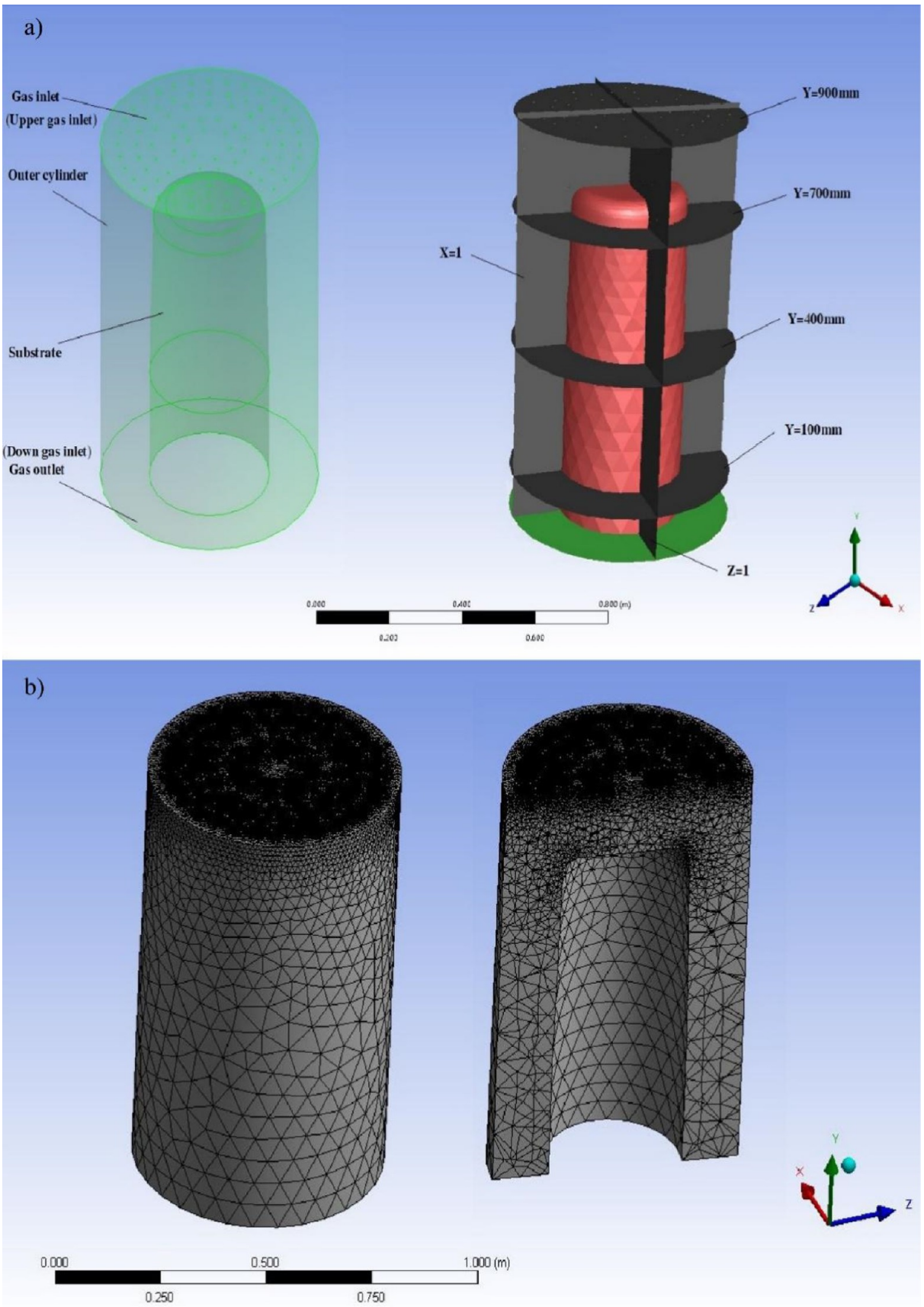

Figure 1. (a) Reactor physical model and (b) meshed model of the reactor vessel.

https://doi.org/10.1021/acsomega.2c04037
ACS Omega 2022, 7, 42044−42055

Table 1. Geometrical Dimensions of the CVD Reactor Model

items	data
height (mm)	920
outer cylinder diameter (mm)	600
susceptor diameter (mm)	300
susceptor height (mm)	750

Table 2. Boundary Conditions of the Meshed Model

Items	data
susceptor heating wall temperature (K)	873
outer cylinder wall initial temperature (K)	300
operating pressure (atm)	1
WF_6 mass flow (L/min)	20
H_2 mass flow (L/min)	60
initial inlet temperature (K)	300

reaction process is simplified and only one step vapor deposition is considered. The influence of surface roughness of the susceptor is not considered. The adsorption and desorption processes of the reaction products are ignored.

2.1. Geometric Model and Grid Sensitivity Analysis. The CVD reactor for the preparation of a tungsten crucible mainly consists of an outer cylinder and a heated susceptor. The external surface of the heated susceptor is the heating surface. It is considered the natural convection heat dissipation on the wall surface of an outer cylinder. There is a sieve plate distributor at the gas inlet of the reactor. In order to simplify the calculation, the hole in the sieve plate distributor is the gas inlet. There is no gas distributor at the gas outlet. Its physical model is shown in Figure 1a. For the convenience of discussion, four cross sections (Y = 100 mm, Y = 400 mm, Y = 700 mm, and Y = 900 mm) and two vertical sections (X = 1 and Y = 1) were selected. The geometric dimensions of the 3D model are shown in Table 1.

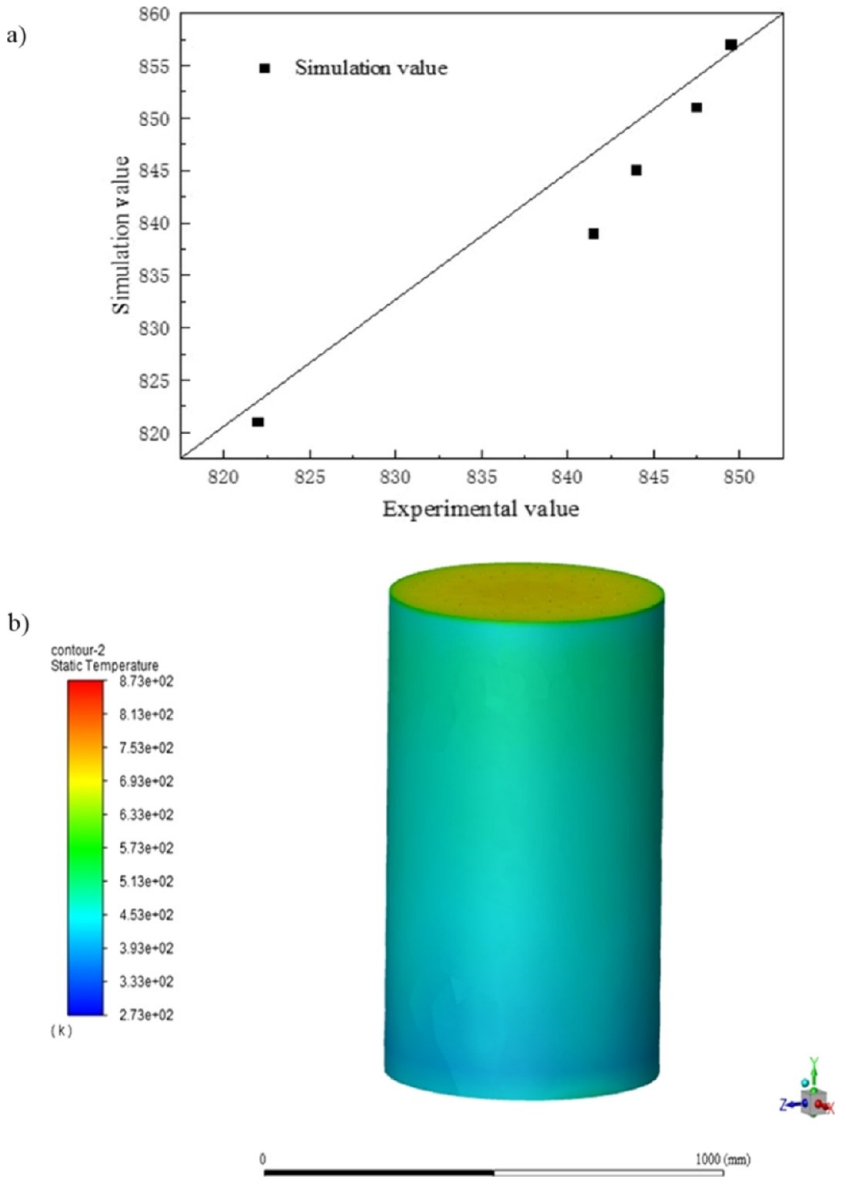

Figure 2. (a) Comparison of simulation results and experimental results and (b) temperature distribution on the cylinder wall of CVD reactor.

https://doi.org/10.1021/acsomega.2c04037
ACS Omega 2022, 7, 42044−42055

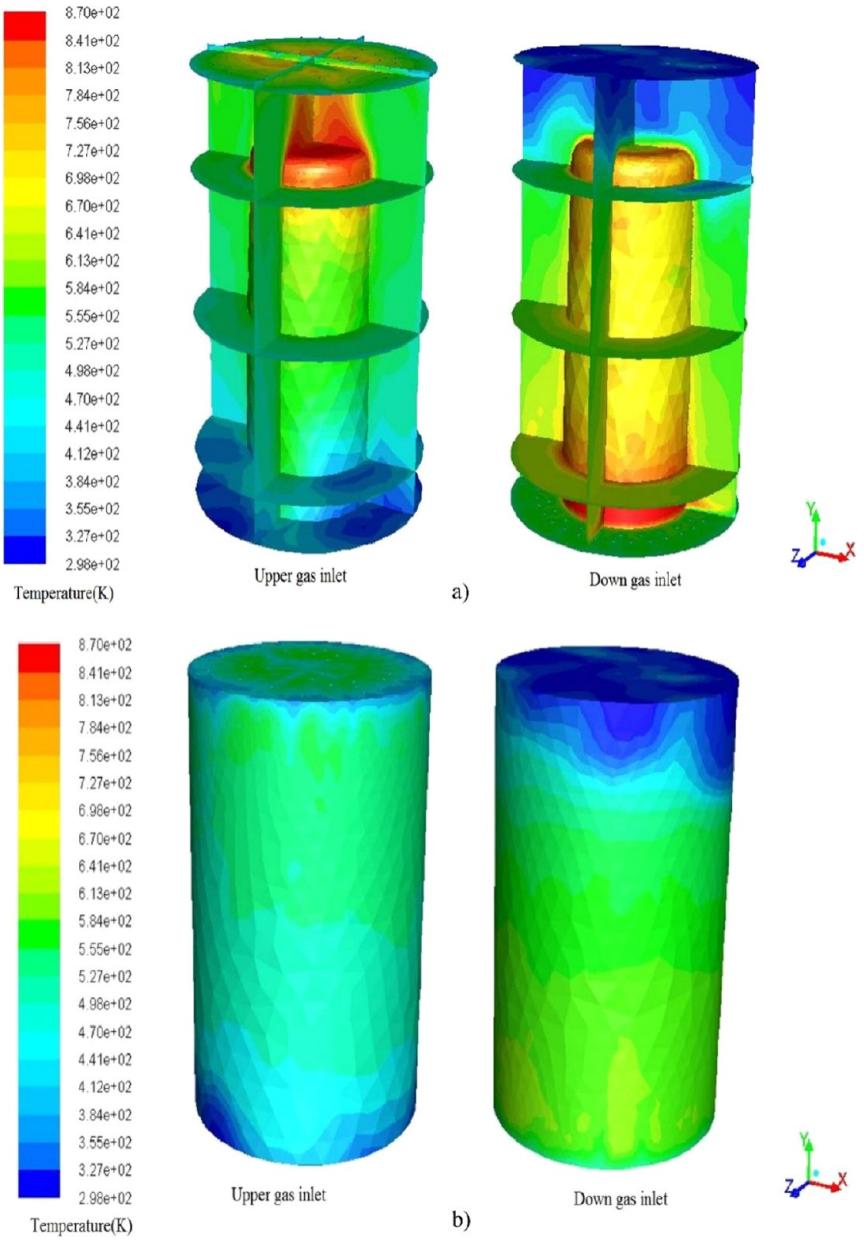

Figure 3. (a) Temperature distribution in a CVD reactor with different gas inlet modes and (b) temperature distribution on the reactor wall with different gas inlet modes.

The 3D CFD model was built and meshed with Ansys Workbench 19.1. An unstructured tetrahedral mesh was used in the fluid domain of the reactor and the mesh was encrypted in the complex structure areas such as the gas inlet. The physical model mesh is shown in Figure 1b. The grid dependency tests are performed for 4 different meshes (grid quantity 1.12, 1.27, 1.36, 1.45, and 1.57 million). The surface temperature of the susceptor in the CVD reactor is chosen as the test parameter. When the grid quantity is 1.57 million, the surface temperature of the susceptor has changed very little. Accordingly, for accuracy and time saving, the mesh (1.57 million) is used for all the simulations.

2.2. Mathematical Model. The tungsten deposition process is a non-steady-state process, as such, the tungsten film thickness changes continuously. Because the growth rate is small, the tungsten film thickness can be considered constant over a short time frame. In this sense, the tungsten deposition process for a given tungsten film thickness can be reasonably simulated in a steady state. Therefore, a series of quasi-steady-state models corresponding to different tungsten film thicknesses were developed, and the governing equations, including continuity, momentum, energy, radiative transport, and chemical species transport equations, are presented in this section.

(1) Community equation

$$\nabla(\rho U) = S \tag{1}$$

where the source term, $S = R_{si}$, is the tungsten deposition rate on the heated susceptor.

Momentum equation

https://doi.org/10.1021/acsomega.2c04037
ACS Omega 2022, 7, 42044−42055

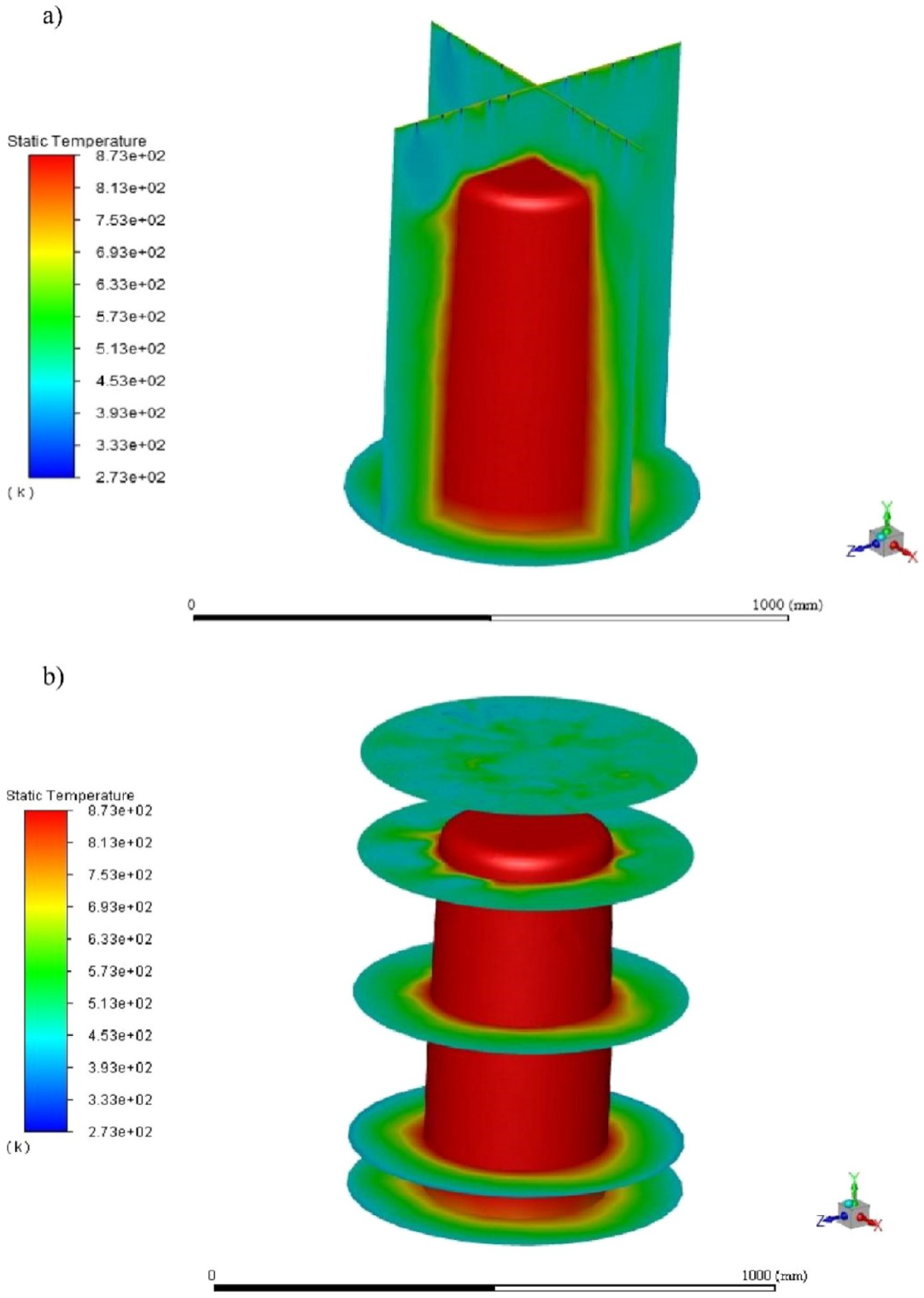

Figure 4. (a) Temperature distribution in the longitudinal section and (b) temperature distribution in the cross section.

$$\nabla(\rho UU) = -\nabla P + \rho g + \nabla\left[\mu\left(\nabla U + (\nabla U)^T - \frac{2}{3}\nabla UI\right)\right] - \nabla(\rho \overline{u}\,\overline{u''}) \quad (2)$$

Because the flow velocity of the reactant gas is small and the Reynolds number is less than 1000, the laminar flow model is adopted for the flow.

(2) Energy equation

$$\nabla[(\rho E + p)U] = \nabla(\lambda_{\text{eff}}\nabla T) + S_{\text{h}} \quad (3)$$

The source term, $S_{\text{h}} = \nabla\bullet[I(r,s)s]$, is the increment of the radiation intensity in direction S.

(3) Radiative transfer equation

$$\nabla\bullet[I(r, s)s] + aI(r, s) = a\frac{\sigma T^4}{\pi} \quad (4)$$

https://doi.org/10.1021/acsomega.2c04037
ACS Omega 2022, 7, 42044−42055

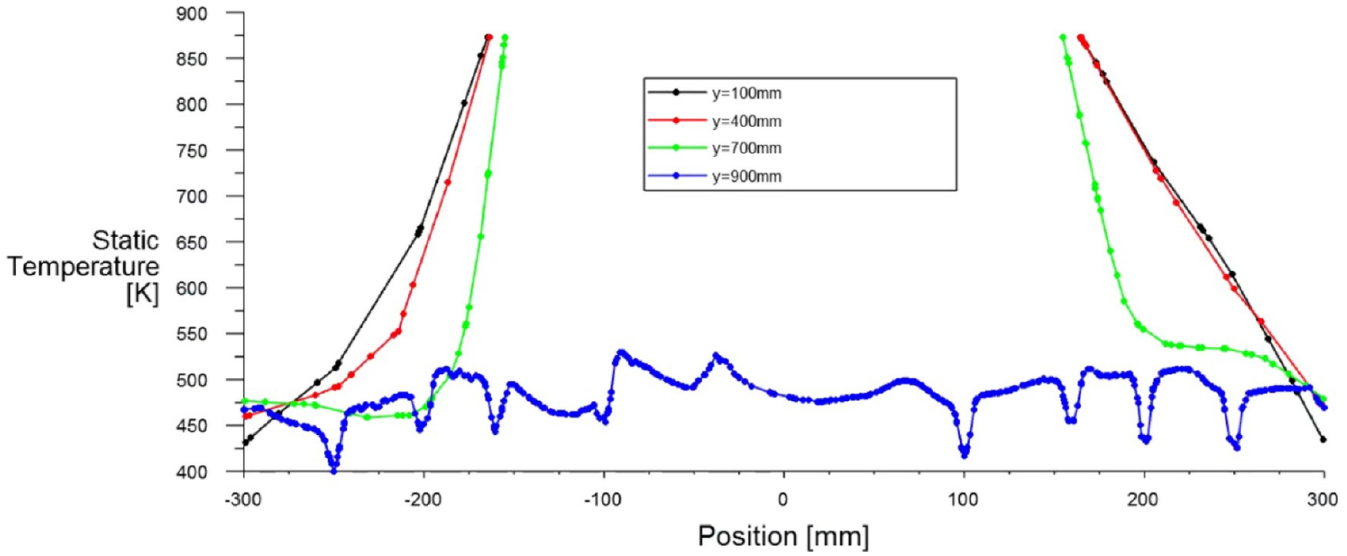

Figure 5. Radial temperature distribution at different heights.

(4) Species transport equations

$$\nabla(\rho U Y_i) = -\nabla J_i(\mathrm{HF},\ H_2,\ WF_6,\ W) \quad (5)$$

$$J_i = -\rho D_{i,j} \nabla Y_i \quad (6)$$

The data for the specific heat, viscosity, and thermal conductivity of the relevant gas species as a function of temperature are given in Reid et al.,[17] and those for the binary diffusion coefficients are estimated using the kinetic theory.[18]

2.3. Simulation Condition. The pressure-based double-precision separation solver of Ansys Fluent 19.1 was used for the simulation calculation. The steady-state flow process with gravity is solved. The coupled algorithm is adopted for pressure−velocity coupling. Momentum equation, energy equation, and discrete radiation equation all adopt the second order upwind scheme. The pressure uses the standard algorithm. The least squares cell-based algorithm was adopted for the gradient equation. The boundary conditions are shown in Table 2.

2.4. Experimental Methodology. The structural dimensions of the experimental setup and the simulated physical model are exactly the same. Twelve temperature measuring points were uniformly arranged on a susceptor. The temperature data were collected by a computer and the surface temperature of the susceptor was calculated. The operating conditions of an experimental reactor and the simulated conditions were kept consistent.

3. RESULTS AND DISCUSSION

3.1. Validation of Computational Fluid Dynamics. The simulation results were compared with the experimental data collected on the surface temperature of the susceptor in the CVD reactor. The simulated value points correspond one-to-one with the experimental temperature measurement points. Moreover, the simulated value point is the average value of the experimental temperature measurement point area. Figure 2a shows that the simulated and experimental values are in good agreement. The simulation error is less than 1%.

The simulation results were compared with the experimental data collected on the surface temperature of the outer cylinder in the CVD reactor. Figure 2b shows the temperature distribution on the outer cylinder wall of the upper gas inlet CVD reactor. It can be seen from the figure that the wall temperature distribution is relatively uniform, with an average temperature of 471 K, which is consistent with an experimental wall temperature of 473 K. This indicates that the model is reliable.

3.2. Effect of Gas Inlet Mode. There are two inlet modes for the mixed gas inlet of the CVD reactor. One way is for the gas to enter the reactor from the top, referred to as the upper gas inlet. The other way is for the gas to come in from the bottom of the reactor, referred to as the down gas inlet. In order to investigate the influence of different gas inlet modes on the flow and heat transfer in the CVD reactor, the temperature field and velocity field distributions of the two modes were simulated and calculated, respectively.

The research results show that the deposition temperature has a significant effect on the chemical vapor deposition rate of tungsten, and the deposition rate will increase with the increase of temperature.[19−21] Therefore, the more uniform the temperature distribution in the reactor, the more uniform the tungsten deposition rate distribution, and the more uniform the tungsten film thickness on the susceptor. Figure 3a compares the three-dimensional temperature distribution in the upper gas inlet mode and the down gas inlet mode. A high-temperature area is formed at the top of the susceptor in the upper intake. The tungsten deposition rate is faster here. The temperature distribution on both sides of the susceptor is relatively uniform, and the tungsten deposition rate is relatively slow, but the deposition rate is relatively uniform. Therefore, in the upper gas inlet, the susceptor will form a thicker tungsten film on the top and a thinner tungsten film on both sides of the susceptor.

Generally speaking, the tungsten deposit thickness is relatively uniform and reasonable. In the down gas inlet, a high-temperature zone is formed near the inlet, where the tungsten deposit rate is faster. The temperature at the top of the susceptor is low and the tungsten deposition rate is relatively slow. When the gas comes in from the bottom, the susceptor will form the opposite. Compared with the upper gas inlet, the tungsten deposit in the down gas inlet is poor, which is not conducive to the preparation of tungsten crucible.

https://doi.org/10.1021/acsomega.2c04037
ACS Omega 2022, 7, 42044−42055

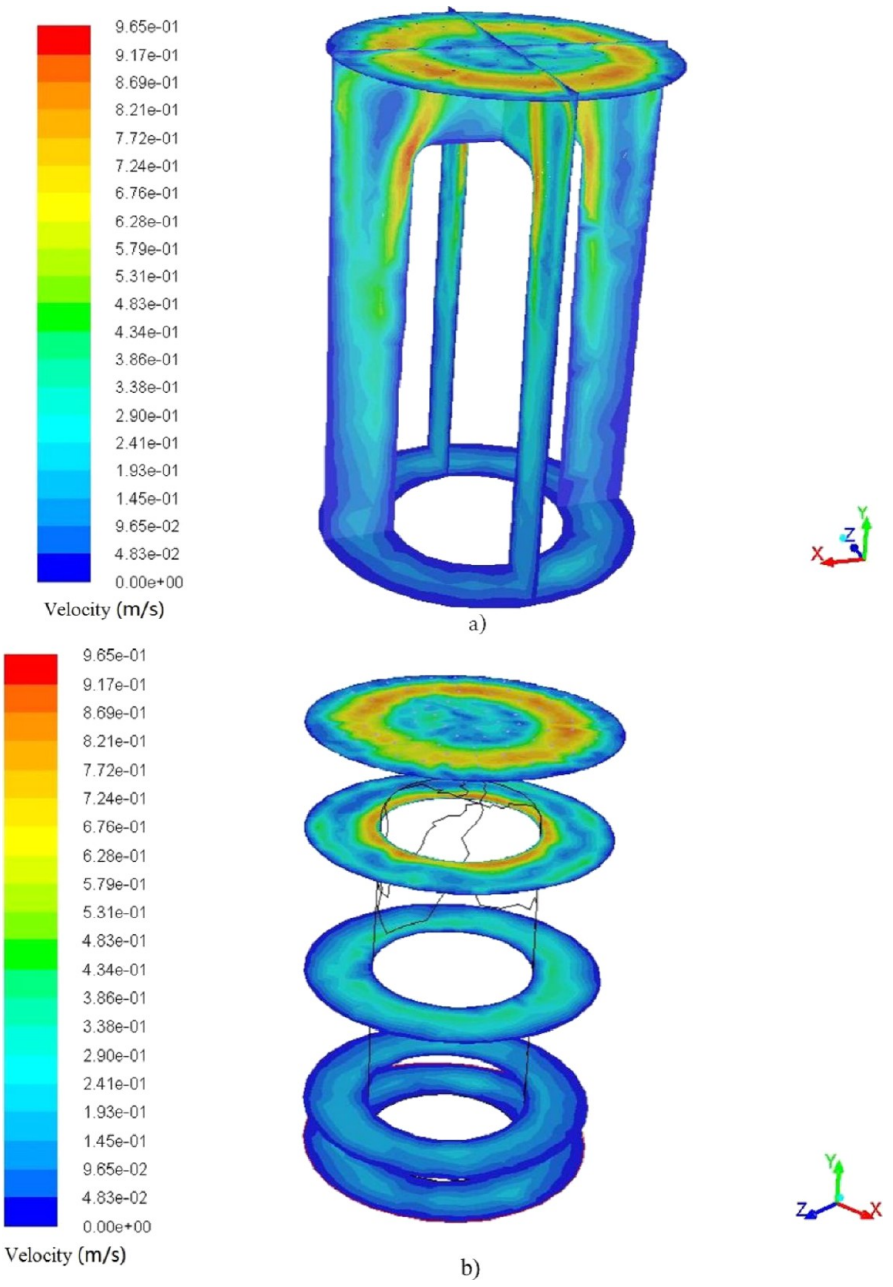

Figure 6. (a) Velocity distribution in the longitudinal section and (b) velocity distribution in the cross section.

Figure 3b compares the temperature distribution on the outer cylinder wall of the reactor in upper and down gas inlets. It can be seen that the temperature distribution on the outer cylinder wall surface is more uniform in the upper gas inlet mode, and the average temperature on the wall surface is lower than that in the down gas inlet mode. This indicates that there is less void deposition of tungsten on the outer cylinder wall in the upper gas inlet mode, which can increase the interest rate of tungsten metal. Generally speaking, the upper gas inlet mode is more favorable to the tungsten deposition process.

3.3. Heat Transfer. The reaction temperature of tungsten hexafluoride produced by hydrogen reduction is relatively low, and the reaction can be carried out under atmospheric pressure. Therefore, the temperature distribution in the CVD reactor is critical. Figure 4a,b shows the temperature distribution of the reactor's longitudinal and cross sections, respectively. The temperature distribution of the reactor in the region between the susceptor and the outer cylinder is relatively uniform, and the temperature at the top of the susceptor is relatively high. This indicates that gas regeneration is slow and convective heat transfer is poor here. The optimal temperature range of tungsten deposition is 673−873 K. The microstructure of the deposition film is a fine columnar crystal with good quality. Therefore, the temperature distribution of the CVD reactor in the upper gas inlet mode completely conforms to the requirement of tungsten deposition reduction reaction.

The radial temperature distribution along the height of the susceptor, as shown in Figure 5, indicates that the temperature distribution near the susceptor is relatively uniform, which also meets the temperature requirements for tungsten deposition. At a height of y = 900 mm, it is farther from the top of the susceptor, so the temperature is lower.

https://doi.org/10.1021/acsomega.2c04037
ACS Omega 2022, 7, 42044−42055

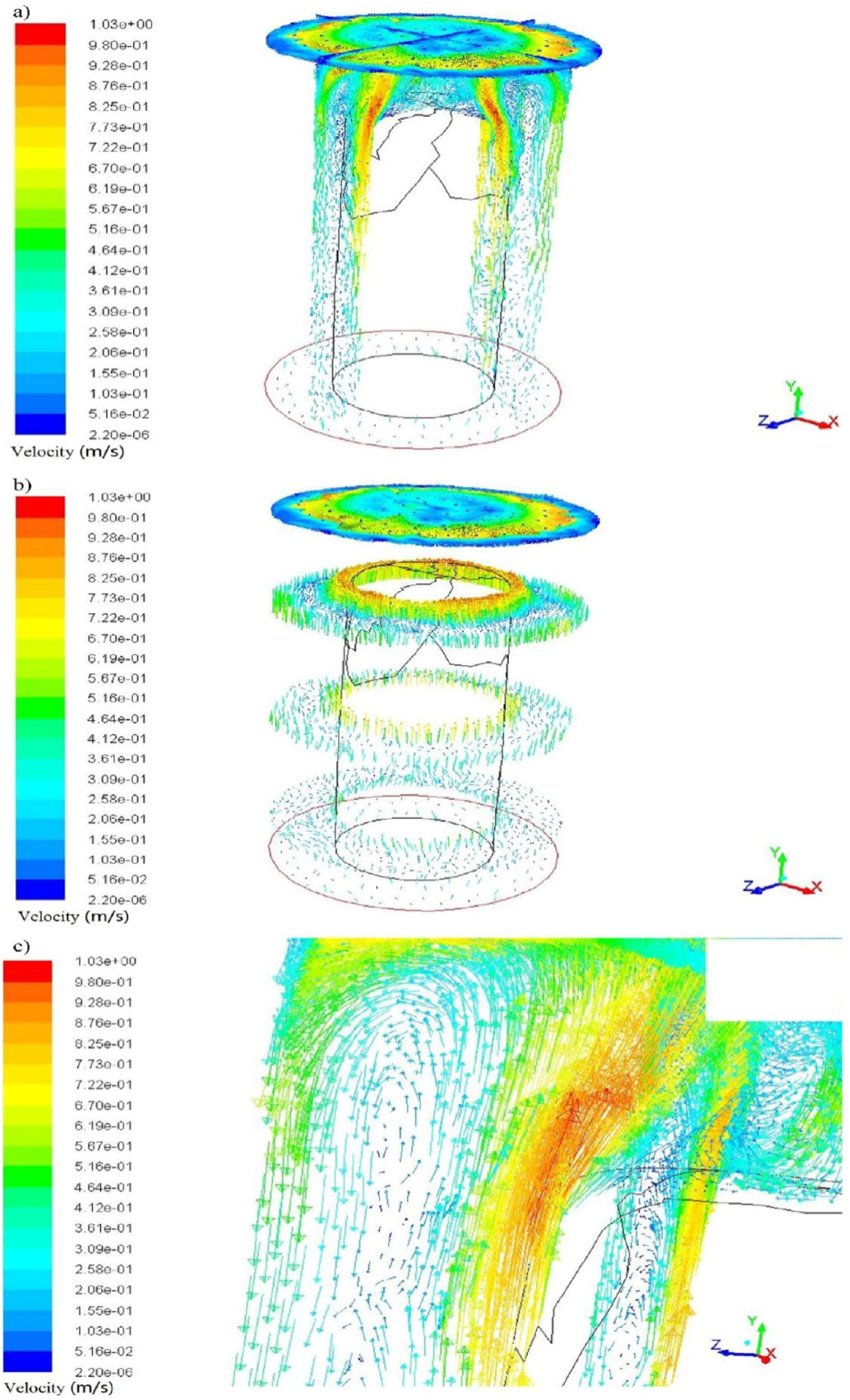

Figure 7. (a) Velocity vector distribution in the longitudinal section, (b) velocity vector distribution in the cross section, and (c) local velocity vector distribution at top edge of the susceptor.

https://doi.org/10.1021/acsomega.2c04037
ACS Omega 2022, 7, 42044−42055

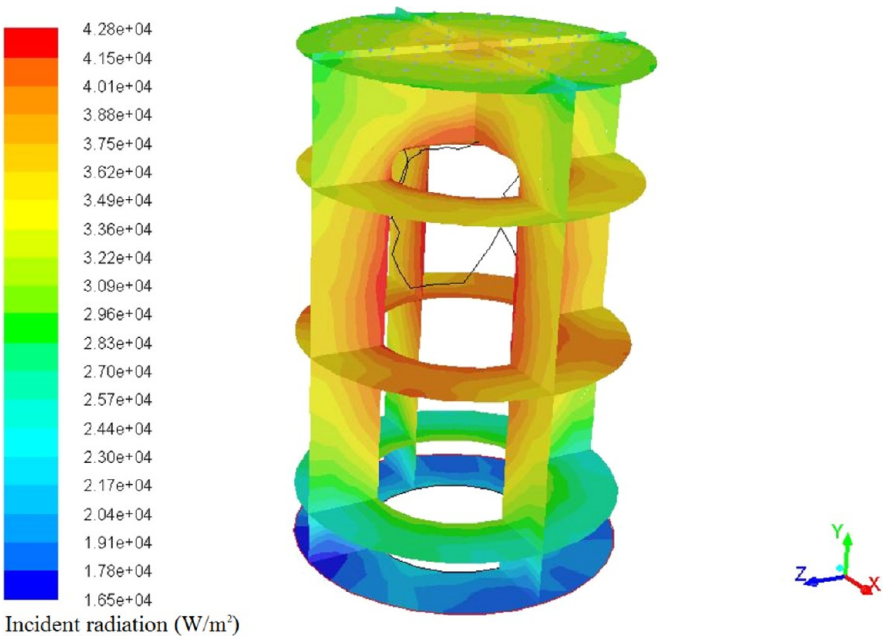

Figure 8. Local velocity vector distribution at top edge of the susceptor.

However, the deposition rate is high at the top and low on both sides of the susceptor, which may cause the problem of uneven thickness of the deposition film. This can be improved by optimizing the reactor structure.

3.4. Flow Characteristics. Figure 6a,b shows the velocity distribution of the longitudinal and cross sections of the CVD reactor. It can be seen that the gas flow velocity at the top edge of the susceptor varies greatly and swirled around the area. A retention zone is formed near the center of the top of the susceptor. Here, the gas velocity is low, the gas renewal is slow. Therefore, this temperature is also higher, and this is also observed in the temperature distribution. In the area between the susceptor and the outer cylinder, the gas velocity distribution tends to be uniform from top to bottom. In the gas outlet, the gas velocity variation tends to be uniform. That is why the temperature distribution in this area is fairly uniform.

Figure 7a shows the velocity vector distribution in the longitudinal section of the CVD reactor. The gas flows downward along the outer cylinder wall area and turns to flow upward in the susceptor wall area. The heat convection between the inside and outside of the main body is formed. Such a convective heat transfer results in a higher temperature in the upper part of the cylinder and a lower temperature in the bottom part.

As can be seen from the cross section velocity vector in Figure 7b, the heat convection also exists in the radial direction of the CVD reactor. The turbulent flow at the top of the susceptor is strong and there are hot whirlpools. Figure 7c can also confirm the above conclusion. The gas flow changes dramatically at the top edge of the susceptor. The mainstream swerves in the region and forms a heat convection.

In summary, the flow characteristics of gases in the CVD reactor also determine the temperature distribution. The velocity distribution is uniform, the convective heat transfer is stable, and the temperature distribution is uniform. Gas turbulence is strong, convective heat transfer is strong, and the temperature is higher.

3.5. Effect of Thermal Radiation. The thermal radiation of CVD reactor mainly comes from the heating surface of the susceptor. Figure 8 shows that the radiation intensity gradually decreases from the middle to both sides of the susceptor. The overall radiation intensity is high. The effect of thermal radiation on the temperature of the CVD reactor cannot be ignored.

3.6. Tungsten Deposition Rate. The tungsten deposition rate is influenced by the excess of H_2 in the reactant. As shown in Figure 9a, when H_2 is insufficient or close to the reactive molar ratio, the tungsten deposition rate is higher, while when hydrogen is excessive, the tungsten deposition rate is relatively low. This indicates that excess hydrogen is not favorable for the tungsten deposition rate. In general, the tungsten deposition rate at the top of the susceptor is higher than that at the side of the susceptor. This may be due to strong gas convection at the top of the susceptor, higher temperature, faster mass-transfer reaction, and higher tungsten deposition rate. The gas convection on the side of the susceptor is weak, the reaction mass transfer is slow, and the tungsten deposition rate is relatively small.

Some scholars believe that formation and diffusion of HF has a certain dilution effect on the initial reactants. Figure 9b compares the concentration distribution of HF generated by the reaction with the tungsten deposition rate distribution. It is found that the tungsten deposition rate is correspondingly lower where the hydrogen fluoride concentration is high. This indicates that if the generated HF is too late to diffuse and escape of the susceptor surface, it will hinder the progress of the deposition reaction and cause the deposition rate to decrease. The diffusion and escape of HF are closely related to the flow of the reactive gas. Therefore, HF expansion and escape process can be enhanced by improving the structure of the reactor and enhancing the gas renewal rate at the susceptor surface, thereby increasing the tungsten deposition rate. Overall, the influence of HF on the deposition of tungsten on the susceptor surface is not the main factor, but the optimization of the reactor structure is still necessary to increase the tungsten deposition rate.

https://doi.org/10.1021/acsomega.2c04037
ACS Omega 2022, 7, 42044−42055

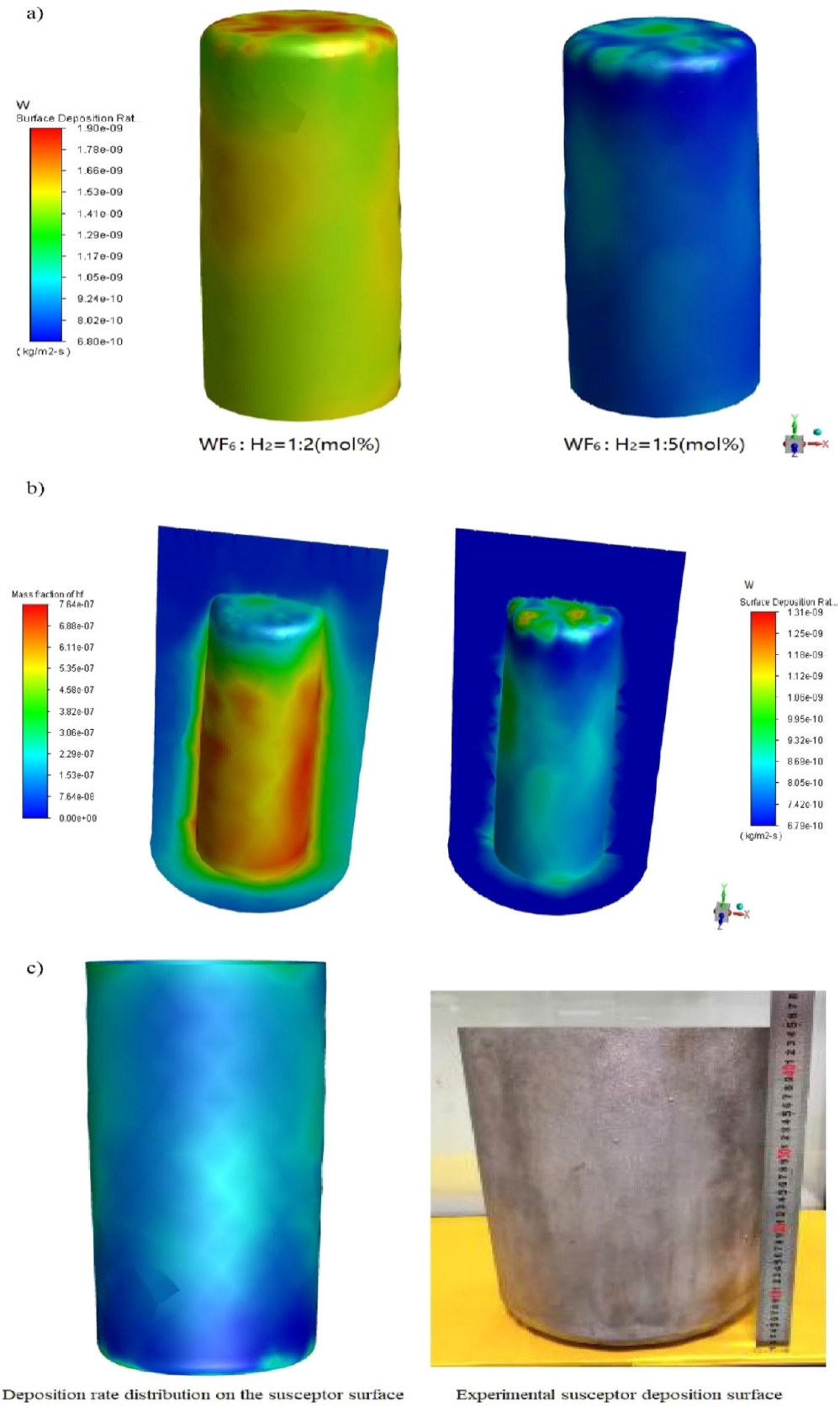

Figure 9. (a) Effect of initial molar ratio of gas on the tungsten deposition rate, (b) effect of HF concentration on the tungsten deposition rate, and (c) simulated tungsten deposition rate distribution vs experimental susceptor surface (photograph courtesy of "Lipei Peng". Copyright 2022).

Generally speaking, where the tungsten deposition rate is high, the film deposited by tungsten is thicker. Figure 9c shows the comparison between the simulated tungsten deposition rate distribution on the susceptor surface and the experimental

https://doi.org/10.1021/acsomega.2c04037
ACS Omega 2022, 7, 42044−42055

susceptor surface morphology, it is found that the distribution characteristics of tungsten deposition rate are similar to the experimental deposition results. This shows that the simulation results have certain guiding significance for future experiments and industrialization.

4. CONCLUSIONS

By the CFD simulation of the tungsten crucible CVD reactor, the velocity distribution and the temperature distribution inside the reactor were obtained. The influence of two gas inlet modes on the temperature distribution of a CVD reactor was compared. It was found that the temperature distribution in the upper gas inlet CVD reactor was more uniform and reasonable, which was more conducive to the deposition process of tungsten. The temperature distribution and velocity distribution of the upper gas inlet CVD reactor were analyzed. It is found that the axial and radial heat convection will form between the susceptor and the outer cylinder. It is just that the axial heat convection is stronger. The molar ratio of H_2 to WF_6 has a great influence on the deposition rate of tungsten, and excess H_2 is not conducive to the deposition of tungsten. The diffusion and escape of HF have a certain effect on the tungsten deposition rate. The simulation results show that the thermal radiation has great influence on the temperature distribution of the CVD reactor, which cannot be ignored. In conclusion, the CFD simulation of CVD reactor can provide guidance for future experiments and industrial design.

AUTHOR INFORMATION

Corresponding Author

Han Dong − *School of Materials Science and Engineering, Shanghai University, Shanghai 200444, China;* orcid.org/0000-0001-9117-0280; Email: qktgzsyx@163.com

Authors

Lipei Peng − *School of Materials Science and Engineering, Shanghai University, Shanghai 200444, China; PERIC Special Gas Co., Ltd, Handan City, Hebei Province 056000, China*

Shaobo Li − *PERIC Special Gas Co., Ltd, Handan City, Hebei Province 056000, China*

Zhanwei Wang − *PERIC Special Gas Co., Ltd, Handan City, Hebei Province 056000, China*

Xiangjun Meng − *PERIC Special Gas Co., Ltd, Handan City, Hebei Province 056000, China*

Yafeng Wang − *PERIC Special Gas Co., Ltd, Handan City, Hebei Province 056000, China*

Tengshi Liu − *PERIC Special Gas Co., Ltd, Handan City, Hebei Province 056000, China*

Xiangyu Li − *PERIC Special Gas Co., Ltd, Handan City, Hebei Province 056000, China*

Jialiang Ji − *PERIC Special Gas Co., Ltd, Handan City, Hebei Province 056000, China*

Complete contact information is available at: https://pubs.acs.org/10.1021/acsomega.2c04037

Funding

This research did not receive any specific grant from funding agencies in the public, commercial, or not-for-profit sectors.

Notes

The authors declare no competing financial interest.

ACKNOWLEDGMENTS

This work was financially supported by PERIC Special Gas Co., Ltd by supplying the equipment and materials.

REFERENCES

(1) Wang, Y.; Yang, X. H.; Bai, L. T. Optimization design of gas distributor for CVD reactor by CFD simulation. *J. Rocket Propul.* **2014**, *40*, 46−51.

(2) Piazza, G.; Matthews, G. F.; Pamela, J.; Altmann, H.; Coad, J. P.; Hirai, T.; Lioure, A.; Maier, H.; Mertens, P.; Philipps, V.; et al. R&D on tungsten plasma facing components for the JET ITER-like wall project. *J. Nucl. Mater.* **2007**, *367*−*370*, 1438−1443.

(3) Hirai, T.; Kreter, A.; Linke, J.; Malzbender, J.; Ohgo, T.; Philipps, V.; Pintsuk, G.; Pospieszczyk, A.; Sakawa, Y.; Sergienko, G.; et al. Critical heat flux loading experiments on CVD-W coating in the TEXTOR tokamak. *Fusion Eng. Des.* **2006**, *81*, 175−180.

(4) Matějíček, J.; Chráska, P.; Linke, J. Thermal Spray Coatings for Fusion Applications—Review. *J. Therm. Spray Technol.* **2007**, *16*, 64−83.

(5) Ying, W. H.; Zhang, H.; Zhang, D. Y. The new development of tungsten and tungsten alloy. *Rare Met. Mater. Eng.* **1990**, *03*, 2−11.

(6) Chen, Z. G.; Yan, B. Y.; Feng, Z. L. Characteristics and Technology Analysis of Tungsten Series Products Produced by Chemical Vapor Deposition. *Rare Met. Cem. Carbides* **2013**, *41*, 17−21.

(7) Lv, Y. W.; Yan, B. Y.; Song, J. P.; Yu, Y. Research Advances and Applications of Tungsten Products via Chemical Vapor Deposition. *China Tungsten Ind.* **2015**, *30*, 53−59.

(8) Bai, S. X.; Niu, D.; Zhu, L. A.; Ye, Y. C. Research Status and Prospect of Preparation of Refractory Metals by Chemical Vapor Deposition. *Cem. Carbide* **2018**, *35*, 381−389.

(9) Chang, I. S.; Hon, M. H. Growth characteristics and electrical resistivity of chemical vapor-deposited tungsten film. *Thin Solid Films* **1998**, *333*, 108−113.

(10) Chang, I. S.; Hon, M. H. Influence of deposition parameters on the texture of chemical vapor Deposit tungsten films by a WF_6/H_2/Ar gas source. *J. Electrochem. Soc.* **1998**, *145*, 3235−3240.

(11) Piglmayer, K.; Schieche, H.; Chabicovsky, R. On the reaction mechanism in laser-induced deposition of tungsten microstructures from WF_6/H_2. *Appl. Surf. Sci.* **2000**, *154*−*155*, 365−368.

(12) Van Veldhuizen, S.; Vuik, C.; Kleijn, C. R. Comparison of numerical methods for transient CVD simulations. *Surf. Coat. Technol.* **2007**, *201*, 8859−8862.

(13) Cheng, W. T.; Li, H. C.; Huang, C. N. Simulation and optimization of silicon thermal CVD through CFD integrating Taguchi method. *Chem. Eng. J.* **2008**, *137*, 603−613.

(14) Ni, H. Y.; Lu, S. J.; Chen, C. X. Modeling and simulation of silicon epitaxial growth in Siemens CVD reactor. *J. Cryst. Growth* **2014**, *404*, 89−99.

(15) Liu, S. S.; Xiao, W. D. CFD−PBM coupled simulation of silicon CVD growth in a fluidized bed reactor: Effect of silane pyrolysis kinetic models. *Chem. Eng. Sci.* **2015**, *127*, 84−94.

(16) Guoqiang, T.; Cong, C.; Yifang, C.; Bing, Z.; Yanguo, C.; Tihu, W. Numerical Simulations of a 96-rod Polysilicon CVD Reactor. *J. Cryst. Growth* **2018**, *489*, 68−71.

(17) Reid, R. C.; Prausnitz, J. M.; Poling, B. E."Viscosity, Thermal Conductivity" in The Properties of Gases and Liquids. 5nd ed.; McGraw-Hill: New York, 1987; pp 9.15−10.34.

(18) Kleijn, C. R.; Kuijlaars, K. J.; Okkerse, M.; van Santen, H.; van den Akker, H. E. A.; et al. Some recent developments in chemical vapor deposition process and equipment modeling. *J. Phys. IV* **1999**, *9*, 117−132.

(19) Ma, J.; Liu, W. W.; Wang, C. Z. Effect of Temperature on Structure and Properties of Tungsten layer Fabricated by Chemical Vapor Deposition. *China Surf. Eng.* **2008**, *05*, 21−25.

(20) Lv, Y. W.; Yu, X. D.; Tan, C. W.; Ma, H. L.; Zheng, J. P.; Wang, F. C.; Cai, H. N. Deposition temperature effects on tungsten single-

crystal layer by chemical vapor transport. *J. Cryst. Growth* **2011**, *329*, 62−66.
(21) Raumann, L.; Coenen, J. W.; Riesch, J.; Mao, Y.; Gietl, H.; Hoschen, T.; Linsmeier, C.; Guillon, O. Modeling and validation of chemical vapor deposition of tungsten for tungsten fiber reinforced tungsten composites. *Surf. Coat. Technol.* **2020**, *381*, 1−29.

https://doi.org/10.1021/acsomega.2c04037
ACS Omega 2022, 7, 42044−42055